

Characterizing early-age and seasonal effects on slab response to environmental loads

J. M. VANDENBOSSCHE, P.E., Ph.D
University of Pittsburgh, Pittsburgh, USA

S. A. WELLS
University of Pittsburgh, Pittsburgh, USA

ABSTRACT: The focus of this study is to provide a detailed analysis on the strain that develops as a result of environmental loads. This study characterizes slab response immediately after construction (first 72 hours after paving) and also addresses seasonal effects over the first two years following construction. A heavily instrumented test section containing both doweled and undoweled slabs was constructed to help better characterize slab response to environmental loads. Surface profile measurements were also made on these slabs at various times of the day during each season. The magnitude of the built-in gradient was quantified along with the early-age response of the slab to environmental loads. It was found that the equivalent linear temperature gradient at the time of set was 0.12 °C/cm (0.22 °F/in). The largest built-in curvature measured along the diagonal for the doweled and undoweled slabs was 0.0000124 1/m (0.0000408 1/ft) and 0.0000138 1/m (0.0000454 1/ft), respectively. The increase in curvature with an increase in equivalent linear temperature gradient for the undoweled slabs was 7 percent higher than the doweled slabs. While the profile measurements are used to quantify overall slab deformation, strain gages were used to analyze the slab response at localized points within the slab. Using strain gages, it was found that a substantial amount of the drying shrinkage occurred within the first 50 days after construction. Despite that the thermal strain was still found to be twice as high as the drying shrinkage the first winter following construction. A thorough characterization of slab response to gradients in the slab is provided. Variations in drying shrinkage and temperature are characterized not only throughout the depth of the slab but also across the slab surface.

KEY WORDS: Curling, warping, gradients, curvature.

1. INTRODUCTION

The trend to move towards a more mechanistic approach in jointed plain concrete pavement (JPCP) design has emphasized the need to more accurately characterize pavement response to environmental and vehicle loads (TRB, 2004). Finite element analysis has been the commonly used tool for calculating pavement stress. It is important to validate these theoretical models with field data since the restraint in thermal- or moisture-related deformation caused by the self weight of the slab, friction between the bottom of the slab and underlying layers, tie and dowel bars and the shoulder are rather complex and difficult to model.

One of the first obstacles to overcome when using finite element to model pavement response is to characterize the magnitude of construction curling and warping that develops in the field (Yu, 2001). Construction curling and warping is the result of a built-in gradient, which occurs as changes in temperature and moisture occur throughout the depth of the slab prior to hardening of the Portland cement concrete (PCC). Slabs that are constructed earlier in the day gain a significant amount of heat energy from solar radiation and hydration of the cement and a positive built-in temperature gradient can develop. At night, the ambient temperature drops and both moisture and heat energy are lost near the surface of the PCC so a negative built-in temperature gradient can develop when slabs are constructed later in the day. The slab remains flat even in the presence of this gradient because the plastic concrete has not developed sufficient stiffness to generate stress or strain. The new Guide for the Design of New and Rehabilitated Pavement Structures (TRB, 2004) has shown the importance of quantifying the built-in gradient on modeling pavement performance (Yu, 2001).

Both pavement instrumentation and direct slab profile measurements are being used to better characterize the effect of temperature and moisture gradients on the performance of concrete pavements [(Jeong, 2001) (Jeong, 2004), (Schmidt, 2000) and (Poblete, 1987)]. This information will be useful to help validate future analytical models. Since stress can not be measured directly, strains are typically measured in the field. Stress develops when the slab is not allowed to expand or contract freely with changes in temperature or moisture content. Stress generated within the slab can be quantified by characterizing the reduction in strain that occurs with changes in moisture content and temperature as a result of the restraint conditions (tie bars, dowel bars, slab-base interface friction or bonding, slab self weight, etc.). The focus of this study is to provide a detailed analysis on the strain that develops as a result of environmental loads and to quantify construction curling and warping for a given set of climate and pavement design conditions. A two-fold approach was adopted for this analysis. While profile measurements of the slab surface provide an overall view of the structural response of the slab, the strain measurements from the instrumented slabs provide information on the response of the slab at discrete points within the slab.

2. DESCRIPTION OF TEST SECTION

A test section was constructed to, among other things, quantify the slab deformation that occurs as a result of environmental loads and the construction curling and warping for a given set of climatic and design factors. The instrumented test section consists of a 30-cm (12-inch) Portland cement jointed plain concrete pavement (JPCP) constructed on top of a 10-cm (4-inch) open-graded asphalt stabilized base, a 13-cm (5-inch) dense-graded subbase, and a 61-cm (24-inch) backfill material, as shown in figure 1. This pavement was constructed on a section of highway on U.S. Route 22 in Murrysville, Pennsylvania (Wells, 2005).

The new JPCP is a four-lane divided highway with 4.6-m (15-foot) transverse joints, 3.7-m (12-foot) lanes, and 0.8-m (2.6-foot) wide concrete curb-and-gutter shoulders. The pavement contained 3.8-cm (1.5-inch) diameter dowels along the transverse joints and 1.6-cm (0.625-inch) diameter tie bars spaced three feet on center along the centerline joint.

The test section is located in the westbound truck lane of Route 22 and consists of seven PCC slabs. The dowel and tie bars were left out of three consecutive slabs so the effect of restraint they impose on the slab could be quantified. A transition slab separates the restrained and unrestrained slabs, as shown in figure 2. Each lane was paved independently using a single-lane slip-form paver. The passing lane was paved several weeks prior to the truck lane, which contained the instrumentation. The layout of the test section can be seen in figure 2.

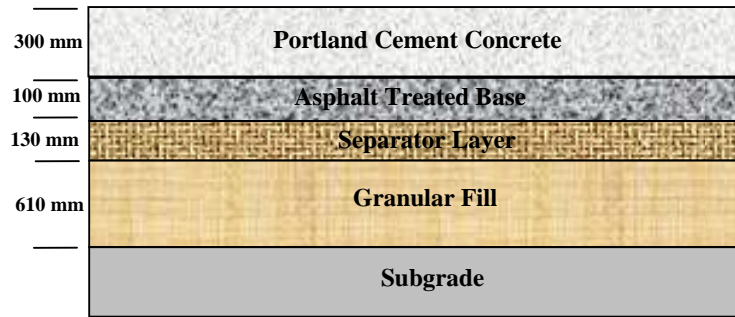


Figure 1: Design thicknesses of the pavement layers.

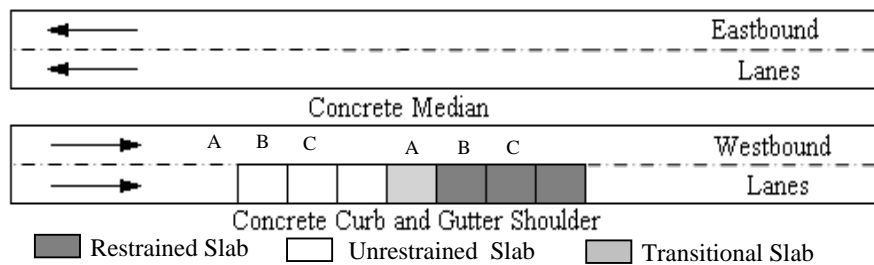


Figure 2: Layout of test section.

3. DESCRIPTION OF RELEVANT INSTRUMENTATION

Figure 3 shows the layout of the instrumentation relevant to this project for both the restrained and unrestrained slabs. The instrumented slabs contain Geokon 4200 vibrating wire static strain gages. The gages are located 25 mm (1 in) from the surface and 25 mm (1 in) from the bottom of the slab. The layout of the gages was replicated for both sets of slabs (restrained and unrestrained). The slabs were also instrumented with temperature sensors. Type T thermocouples were installed at various depths throughout the concrete and throughout the pavement structure to accurately quantify thermal gradients. The thermocouples were installed in the restrained slabs at midpanel and at the corner of the slab in two replicate locations. Wind speed, temperature and relative humidity were measured in the field using an on-site weather.

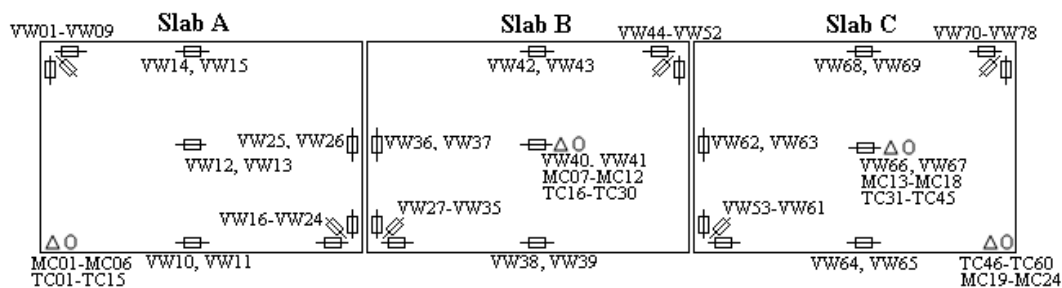


Figure 3: Instrumentation layout of test section.

4. NONLINEAR TEMPERATURE GRADIENTS

The temperature gradients described earlier are calculated simply by dividing the temperature at the top and the bottom of the pavement by the distance between them. The shortcoming of this method is that it provides a linear relationship while non-linear gradients are known to exist in the pavement. In order to account for the non-linear temperature gradients, the parameter "temperature moment" was developed by Janssen and Snyder (2000). The temperature moment was developed so that a nonlinear gradient can be equated to an equivalent linear gradient based on an equivalent strain condition. Temperature moment can be calculated using equations 1 and 2. The temperature moment can then be used to find the equivalent linear temperature gradient based on an equivalent strain using equation 3.

$$TMo = -0.25 \sum_{i=1}^n [(t_i + t_{i+1})(d_i^2 - d_{i+1}^2) - 2(d_1^2 - d_n^2)T_{wave}] \quad \text{Equation 1}$$

TMo = Temperature moment

t_i = Temperature at location i

d_i = Depth at location i

T_{wave} = Weighted average temperature (see equation 2)

$$T_{wave} = \sum_{i=1}^n \left[\frac{(0.5)(t_i - t_{i+1})(d_i + d_{i+1})}{(d_1 - d_n)} \right] \quad \text{Equation 2}$$

$$ELG = -\frac{12(TMo)}{h^3} \quad \text{Equation 3}$$

ELG = Equivalent linear gradient

h = Slab thickness

5. BUILT-IN CONSTRUCTION CURLING AND WARPING

The instrumented pavement was paved on August 1, 2004 at approximately 7:00 AM. Figure 4 shows the temperature distribution throughout the pavement and sublayers at the time of paving, setting, and joint cracking. The estimated time of set of 10 hours was based on static strain measurements. Figure 4 shows strain versus change in temperature. The set time was defined as the time strain began to develop with changes in temperature. This was also about the same time the joints were sawed. At the time of set, there was an equivalent linear gradient of 0.17° C/cm (0.44 °F/in) at the edge and 0.12 °C/cm (0.22 °F/in) at midpanel. The joints cracked approximately 17 to 19 hours after paving when a large negative gradient of about -0.61 °C/cm (-1.10 °F/in) was in present, as shown in figure 5. Figures 5 and 6 show the temperature distribution at midpanel and the edge of the slab, respectively. These graphs illustrate the fact that the temperature distribution throughout the slab is not uniform so the deformation produced by the temperature gradients in the slab will not be symmetrical. This phenomena has been reported by previous researchers, including Jeong and Zollinger (2001).

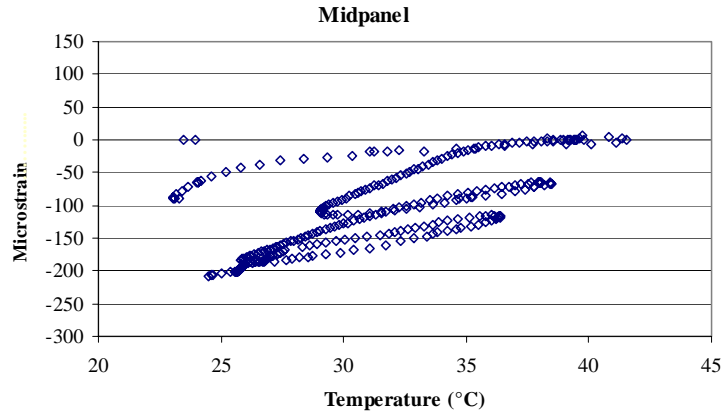


Figure 4: Strain versus temperature at midpanel for the first 72 hrs after paving.

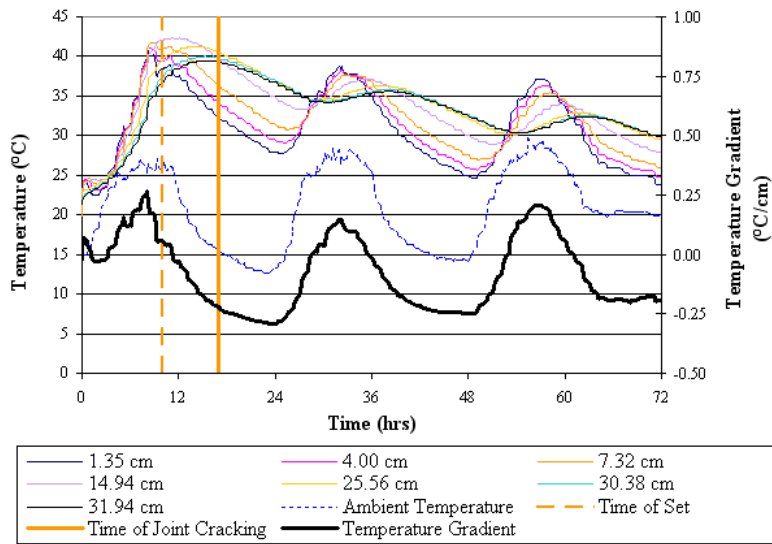


Figure 5: Temperature distribution and gradients at slab midpanel.

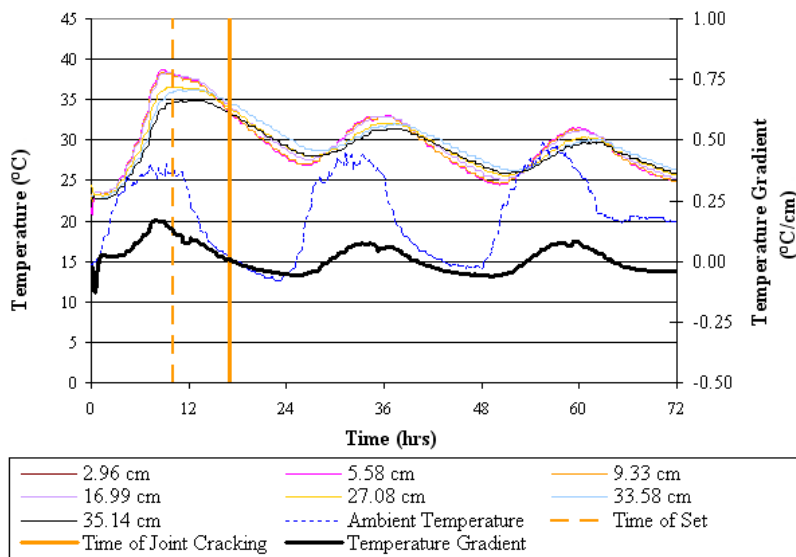


Figure 6: Temperature distribution and gradients at slab edge.

6. SURFACE PROFILE MEASUREMENTS

In order to quantify the effect of early-age (first 72 hours) effects of curling and warping on concrete pavements, surface profile measurements are taken. These profile measurements capture the shape of the slab under various temperature and moisture gradients. In order to measure the surface profiles of slabs experiencing thermal and moisture gradients, an instrument called a Dipstick, manufactured by Face Construction Technologies, Inc. was utilized. The Dipstick pictured in figure 7.a, is a highly sensitive device that measures difference in elevation between successive points along a surface. When walked across a slab, relative elevations of the slab profile, and hence curling and warping can be measured. Surface profiles were measured across the slab in the longitudinal, diagonal, and transverse directions, as outlined in figure 7.c.

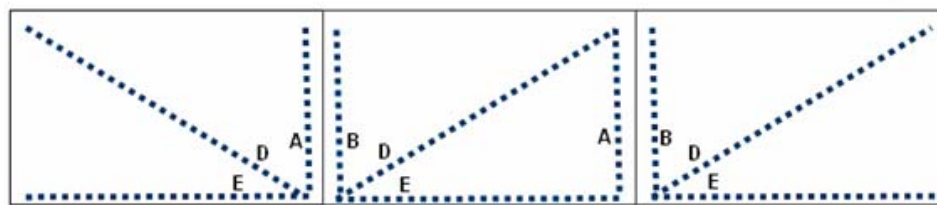
Note the two circular objects located near the transverse joints along the shoulder in figure 7.c. These objects represent the tops of invar rods which were placed in the ground at a depth of approximately 3.7 m (12 feet). In order to further insure the consistency of this reference elevation, the upper portion of the invar rods were encased in grease-filled polyvinylchloride (PVC) tubing in order to protect the rods from the expansive stresses induced by frost exposure. The top of this rod, pictured in figure 7.b, maintains a constant elevation throughout the year and is thus used as a benchmark for all slab profile measurements. Initiating each dipstick run off from the top of the rod allows all relative elevations measured with the dipstick to be tied into actual elevations. Note that imperfections in the slab were taken into account by zeroing each profile based on the time the concrete set.



a. Dipstick



b. Invar rod



c. Surface profile measurement locations

FIGURE 7: Surface profile measurement paths.

The dipstick was able to provide a dynamic representation of the concrete slab surface profile as daily temperature moments caused it to curl. The main focus of this analysis was to evaluate the curling response to different joint conditions, in particular between those with and without dowel and tie bars.

Representative slab profiles measured in the transverse direction are shown in figure 8 and 9. Profiles measured along the longitudinal and diagonal were not included due to space restrictions but can be found in reference by Wells (2005). The figure contains

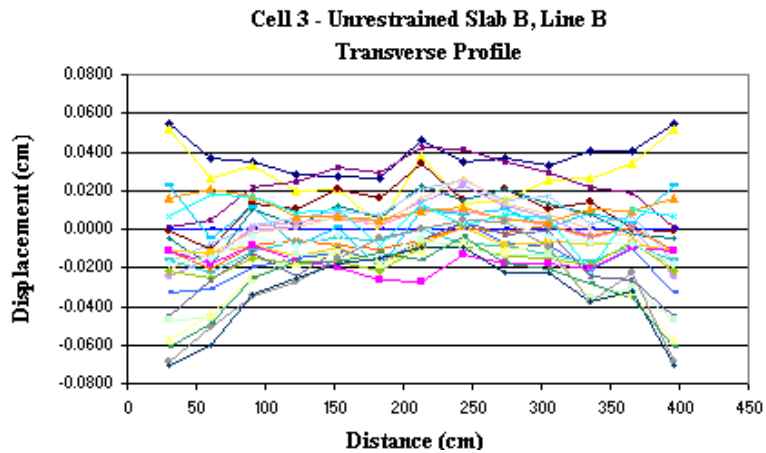


FIGURE 8: Transverse profiles for an unrestrained slab.

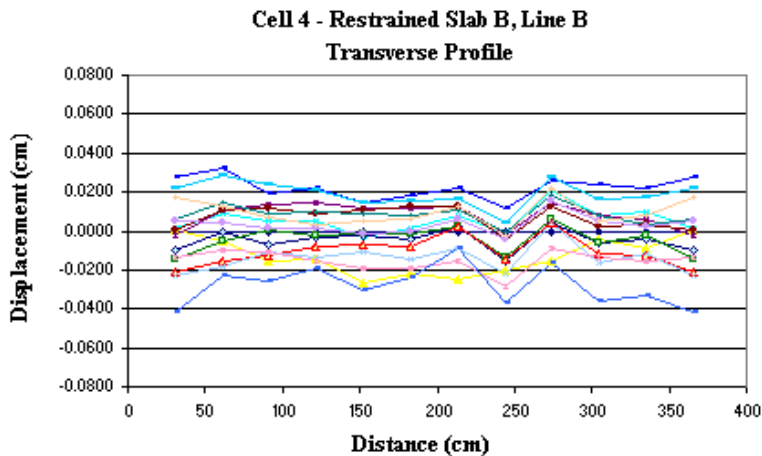


FIGURE 9: Transverse profiles for a restrained slab.

profiles measured at different times of the day for both the restrained (slabs containing dowel and tie bars) and unrestrained (slabs without dowel or tie bars) slabs. All profiles presented here were measured within the first week after paving prior to the placement of the curb and gutter.

As would be expected, the maximum displacement for the unrestrained slab was substantially higher than the restrained slab. The movement of the end of an unrestrained slab as a result of curling and warping can be as much as twice as high compared to the restrained slab.

7.0 SLAB CURVATURE BEFORE AND AFTER THE JOINTS CRACK

The curvature for each profile was then calculated by fitting a second order polynomial to the measured profile. The curvature of the polynomial was calculated one foot into the slab from the shoulder. By combining the profile data with the equivalent linear gradient derived from the midpanel thermocouples, the relationship between slab curvature and equivalent linear temperature can be established.

The response of the slab to temperature gradients before and after the joints crack is quite different, as would be expected since the effective slab length is substantially longer. Figure

10 shows the curvature calculated for profiles measured before and after the joints cracked for Slab A (see figure 2) in the unrestrained cell. The curvature calculated before the joints cracked (shown as solid circles) are well below the best fit line of all of the data points. In all cases except when the equivalent linear gradient is quite high, curvature calculated before cracking will be less than curvature calculated after cracking by a factor of two.

The largest built in curvature measured along the diagonal for the restrained and unrestrained slabs was 0.0000124 1/m (0.0000408 1/ft) and 0.0000138 1/m (0.0000454 1/ft), respectively. The average built in curvature for the restrained slabs was 0.0000103 1/m (0.0000337 1/ft) with a standard deviation of 0.00000263 1/m (0.00000864 1/ft). The average built in curvature for the unrestrained slabs was 0.0000123 1/m (0.0000405 1/ft) with a standard deviation of 0.00000142 1/m (0.00000465 1/ft).

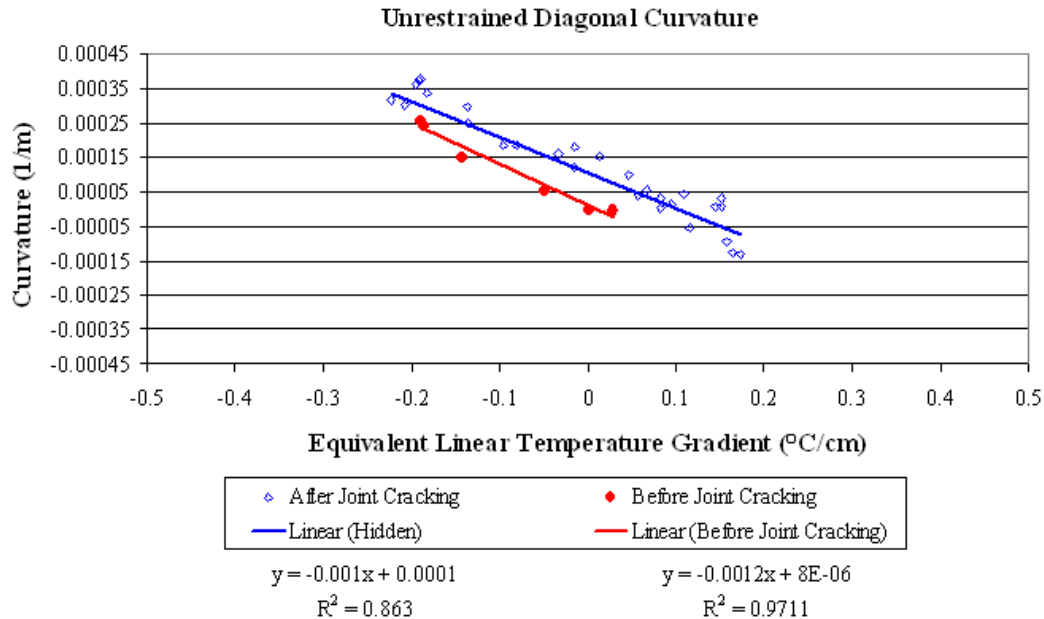


FIGURE 10: Illustration of the relationship between equivalent linear temperature gradient and curvature before and after joint cracking for the diagonal profiles of the unrestrained cell.

8.0 EFFECT OF MIDPANEL TEMPERATURE ON SLAB CURVATURE

Figures 11 and 12 illustrate the relationship between curvatures for the diagonal profiles measured for the unrestrained and restrained slabs and equivalent linear temperature gradient. Only the curvatures calculated for the profiles measured after the slab cracked were used to generate the plots.

In this analysis, the slope of the line indicates the rate of increase in curvature with an increase in equivalent linear temperature gradient. The slopes of the restrained profiles are on average 7 percent less than those of the unrestrained. The maximum curvatures for the restrained slab are also substantially less than the unrestrained. The reduction in curvature for the restrained slab provides an indication of the stress that develops within the slab when this curvature is restrained.

The y-intercept is dependent on the time the slab set and the resulting curvature set into the slab (built in curvature). In other words, it is the curvature present when a temperature gradient is not present in the slab. This will be a function of the time each slab was paved, the temperature gradients that developed throughout the day and the restraint conditions.

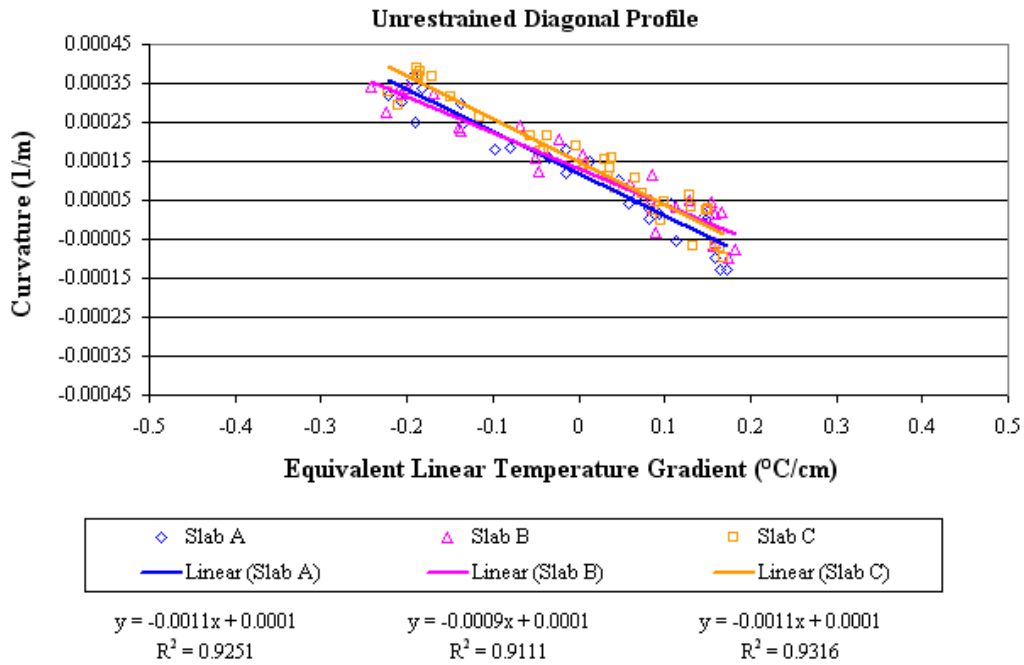


FIGURE 11: Equivalent linear temperature gradient versus curvature for diagonal profiles at unrestrained slabs.

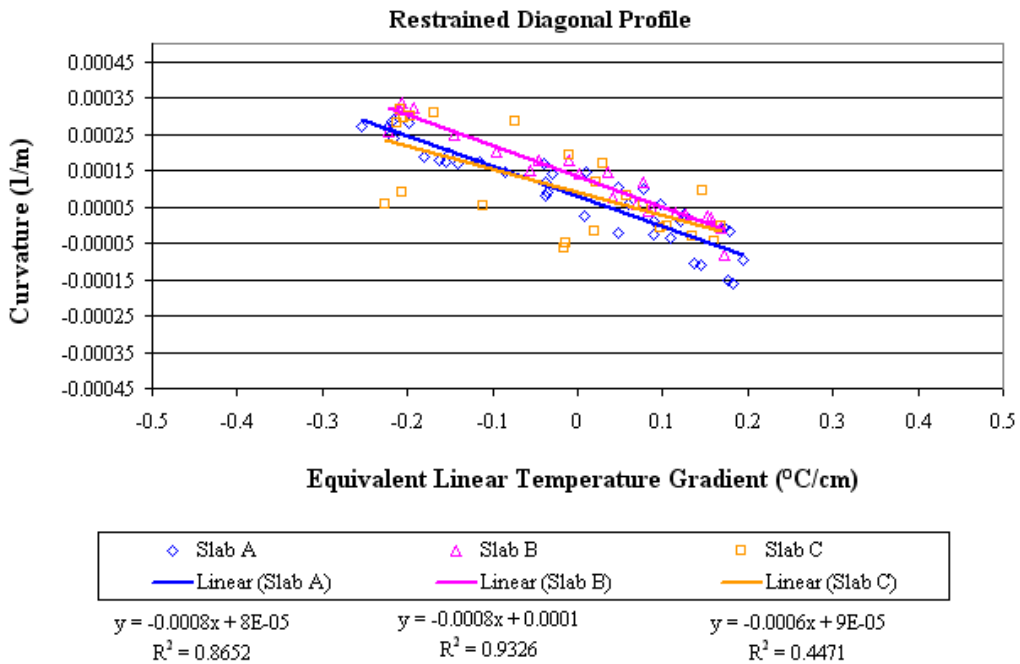


FIGURE 12: Equivalent linear temperature gradient versus curvature for diagonal profiles at restrained slabs.

9.0 EFFECT OF MIDPANEL TEMPERATURE ON SLAB CURVATURE

While the profile measurements are used to quantify overall slab deformation, strain gages were used to analyze the slab response at localized points within the slab. The measured strains along with equation 4 are used to quantify the effects of creep and changes in temperature and moisture in the slab.

$$\mu_{m,c,t} = (R_1 - R_0)B + (T_1 - T_0)(C_1) \quad \text{Equation 4}$$

$\mu_{m,c,t}$ = strain influenced by creep, moisture, and temperature changes

R_0 = raw strain at time 0 (initial concrete set)

R_1 = raw strain at time 1

T_0 = temperature at time 0 (initial concrete set)

T_1 = temperature at time 1

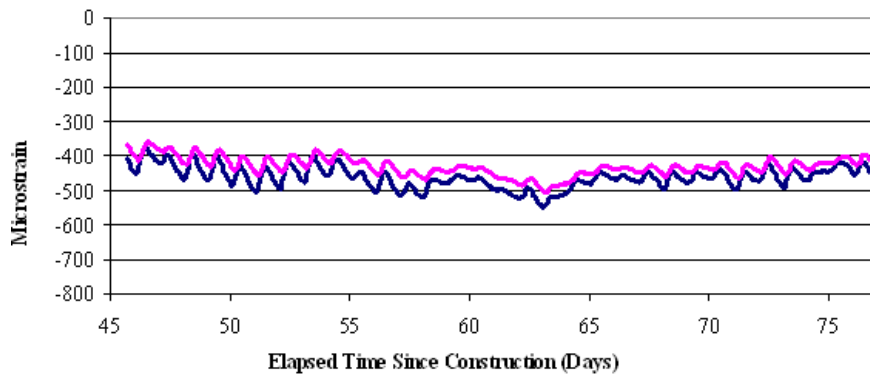
C_1 = thermal coefficient of expansion of steel in strain gage
= 6.78 microstrain/°F

B = batch calibration factor (provided by the manufacturer)

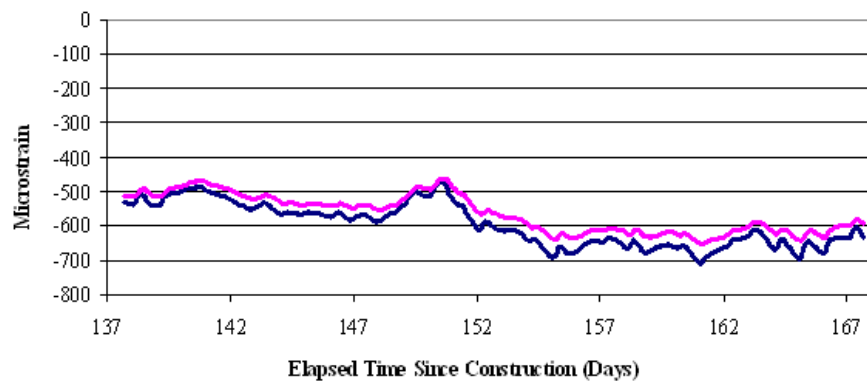
Figure 13 is a plot of the strain measured in the longitudinal direction along the lane/shoulder joint for an unrestrained slab. The strain measured in October, shortly (2 months) after construction because the temperature throughout the depth of slab at the time of set is higher than the slab temperatures typically encountered during the month of October. The strain at the top of the unrestrained slab is greater than that at the bottom due to the higher degree of drying shrinkage that takes place at the surface compared to the bottom of the slab.

As ambient temperatures drop in the winter, the measured strains become increasingly negative as indicated by figure 13.b. The average strain in the following fall was around -450 microstrain while the average strain in the winter was -600 microstrain. The diurnal temperature swings also decrease in the winter due to prevailing seasonal temperature patterns and length of daylight hours. This produces a decrease in diurnal strain fluctuations for the strains measured in the fall (figure 13.a) compared to those measured in the winter (figure 13.b). The drying shrinkage at the surface of the slab also appeared to be slightly higher in the winter than the fall. Factors contributing to this are the humidity in the winter is lower and there are fewer precipitation events. Plus, a substantial amount of drying shrinkage will occur the first 90 days after construction.

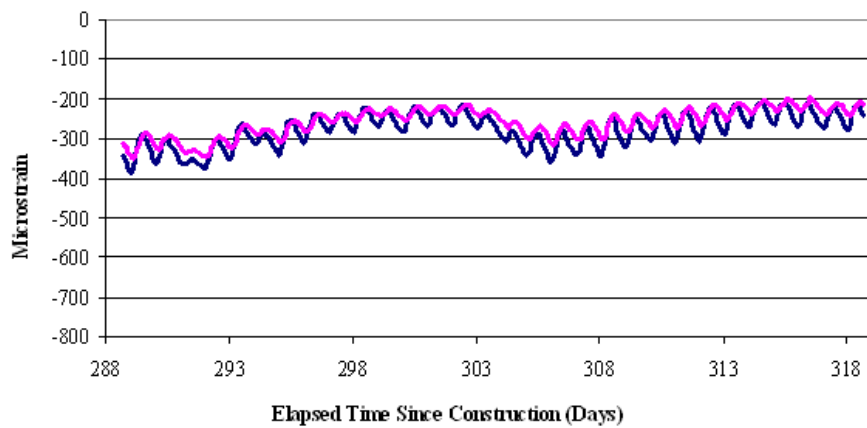
Strains measured in the summer (June) are shown in figure 13.c. The ambient temperatures increase during the spring and summer. This resulted in a decrease in the average strain from -600 microstrain in the winter to -250 microstrain in the spring and early summer. Figure 13.c shows that the daily strain fluctuations are also much larger in the summer than in the winter (figure 13.b). The reason for this can be contributed to the fact that there are higher temperature fluctuations in the spring and summer. These temperature fluctuations are much larger on the surface than the bottom of the slab and this is reflected in the larger strain fluctuations measured on the surface of the slab.



a. Fall



b. Winter



c. Summer

FIGURE 14: Static strain measured along the lane/shoulder joint for an unrestrained slab.

10.0 EFFECTS OF DRYING SHRINKAGE AND CREEP ON STRAIN (FIRST TEN MONTHS AFTER PAVING)

The following section provides a look at the effects of moisture-related shrinkage, creep and the restraint conditions at locations within the slab throughout the year. These components are isolated from temperature-induced strain in this analysis using equation 4.

$$\mu_{m,c} = (R_1 - R_0)B + (T_1 - T_0)(C_1 - C_2) \quad \text{Equation 5.}$$

$\mu_{m,c}$ = strain influenced by creep and moisture changes
 R_0 = raw strain at time₀ (initial concrete set)
 R_1 = raw strain at time₁
 T_0 = temperature at time₀
 T_1 = temperature at time₁
 C_1 = thermal coefficient of expansion of steel in strain gage (6.78 microstrain/°F)
 C_2 = thermal coefficient of expansion of the concrete (5.71 microstrain /°F, measured in the laboratory)
 B = batch calibration factor (provided by the manufacturer)

Note that this equation is similar to equation 5; however, the effects of thermal strain are removed by subtracting out the thermal expansion of the concrete. Figure 14 provides a direct comparison between the contributions of temperature-related; moisture-related changes, creep and restraint conditions; moisture- and temperature-related changes, creep and restraint to strain development. The strains in figure 14 are the average of strains measured from three different slabs 25 mm (1 in) from the surface.

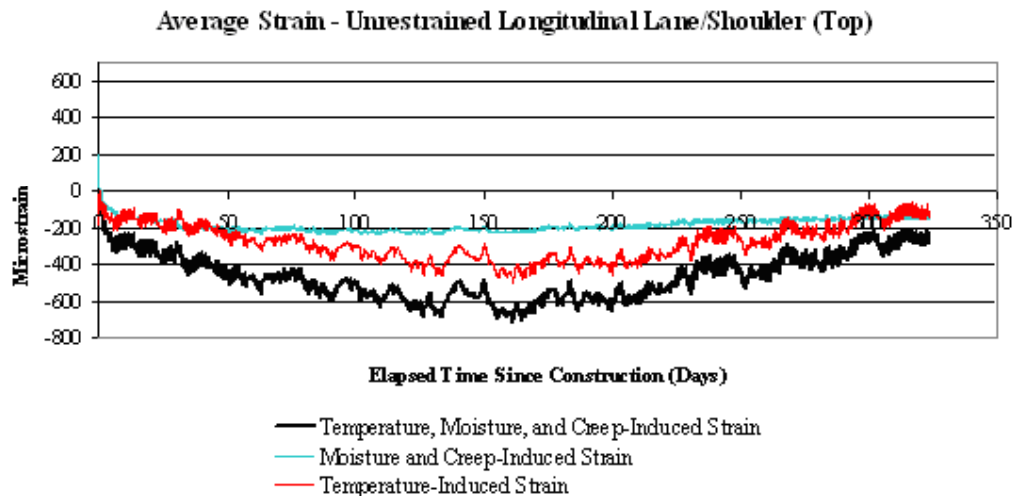


FIGURE 14: Contribution of temperature, creep, and drying shrinkage on total strain.

Temperature was shown to have the greatest effect on strain throughout the year. From the time of construction, the temperature induced strain follows the seasonal ambient temperature trend and the magnitude of strain steadily increased until reaching a maximum in the winter. The strain decreases as the ambient temperatures increase in the spring and summer.

Moisture-related shrinkage is typically less than thermal strain. From figure 14, thermal strain was found to be twice as high as the moisture-related shrinkage the first winter after

construction. Moisture-related shrinkage is influenced by relative humidity, but unlike temperature, relative humidity does not experience pronounced diurnal fluctuations. In general, the moisture-related shrinkage increases drastically the first 50 days after construction. The increase in moisture-related shrinkage continues through the winter months but then begins to decrease during the spring when precipitation events occur more frequently. This gradual lessening of moisture-related shrinkage (reversible drying shrinkage) can be seen in figure 15 in the range of 150 to 250 days after construction. This phenomenon makes it possible to determine the magnitude of reversible shrinkage that will occur throughout the slab. For the restrained slabs, the moisture-related shrinkage along the centerline was closer to the moisture-related shrinkage at midpanel for the restrained slab compared to the unrestrained slab. This is because the tie bars keep the centerline joint tight and reduce the exposure to the ambient air and wind.

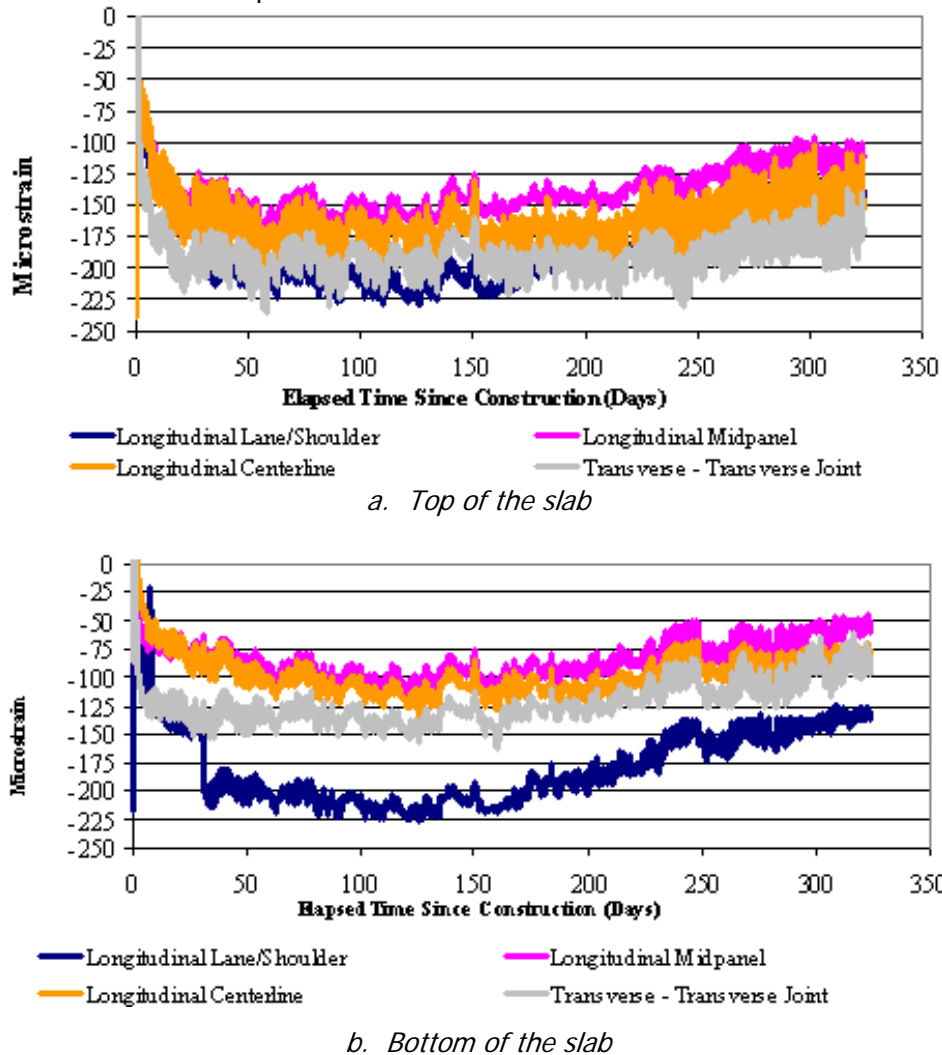


FIGURE 15: Drying shrinkage and creep at locations throughout an unrestrained slab.

11.0 CONCLUSIONS

The magnitude of the built-in gradient was quantified along with the early-age response of the slab to environmental loads. It was found that the equivalent linear temperature

gradient at the time of set was 0.12 °C/cm (0.22 °F/in). The largest built-in curvature measured along the diagonal for the doweled and undoweled slabs was 0.0000124 1/m (0.0000408 1/ft) and 0.0000138 1/m (0.0000454 1/ft), respectively. The increase in curvature with an increase in equivalent linear temperature gradient for the undoweled slabs was 7 percent higher than the doweled slabs. While the profile measurements are used to quantify overall slab deformation, strain gages were used to analyze the slab response at localized points within the slab. Using strain gages, it was found that a substantial amount of the drying shrinkage occurred within the first 50 days after construction. Despite that the thermal strain was still found to be twice as high as the drying shrinkage the first winter following construction.

ACKNOWLEDGEMENTS

The authors would like to thank the Pennsylvania Department of Transportation (PENNDOT) and the Federal Highway Administration (FHWA) for their financial and technical support. In addition the authors would like to thank all the graduate and undergraduate students who assisted in the completion of this project.

REFERENCES

Choubane, B. and M. Tia, "Nonlinear temperature gradient effect on maximum warping stresses in rigid pavements," *Transportation Research Record 1370*, Washington, DC, 1992, pp. 65-71.

Grasley, Z. C., D. A. Lange and M.D. D'Ambrosia, "Internal relative humidity and drying stress gradients in concrete," *Proceedings of Engineering Conferences International, Advances in Cement and Concrete IX*, Copper Mountain, CO, 2003.

Hveem, F. N., "Slab warping affects pavement joint performance," *Journal of the American Concrete Institute*, Vol. 22, No. 10, *Proceedings V. 47*, June 1951.

Janssen, D. J. and M. B. Snyder, "The Temperature-moment concept for evaluating pavement temperature data. Technical note." *Journal of Infrastructure Engineering*, Vol. 6, No. 2. American Society of Civil Engineers. Reston, VA, June 2000, pp. 81-83.

Janssen, D. "Moisture in portland cement concrete," *Transportation Research Record 1121*, National Research Council, Washington, DC, 1987, p 40-44.

Jeong, J. H., L. Wang and D. G. Zollinger, "A temperature and moisture module for hydrating Portland cement concrete pavements," 7th International Conference on Concrete Pavements, Orlando, FL, September 2001, pp. 9-22.

Jeong, J. H. and Zollinger, D. G. "Early-age curling and warping behavior: insights from a fully instrumented test-slab system," *Transportation Research Record 1896*, National Research Council, Washington, DC, 2004, pp. 66-74.

Poblete, M., R. Salsilli, A. Valenzuela and P. Spratz, "Field evaluation of thermal deformation in undoweled PCC pavement slabs," *Transportation Research Record 1207*, National Research Council, Washington, DC, 1987, pp. 217-228.

Reddy, A. S., G. A. Leonards, and M. E. Harr, "Warping stresses and deflections in concrete pavements: Part III," *Highway Research Record No. 44*, Washington, DC, 1963.

Schmidt, Sarah, *Built-In Curling and Warping in PCC Pavements*, M.S. Thesis, University of Minnesota, 2000.

Transportation Research Board, National Research Council, Guide for Mechanistic-Empirical Design of New and Rehabilitated Pavement Structures- Final Report, National Cooperative Highway Research Program 1-37A, March 2004.

Vandenbossche, J. M. and M. B. Snyder, "Comparison between measured slab profiles of curled pavements and profiles generated using the finite element method," *8th International Conference on Concrete Pavements*, Denver, CO, August 2005, pp. 1155-1172.

Wells, S. A., B. M. Phillips, J. M. Vandenbossche, "S.R.-22 smart pavement phase I: early-age material properties and pavement response characteristics for jointed plain concrete pavements, Phase I Final Report", submitted to the Pennsylvania Department of Transportation and the Federal Highway Administration, June 2005.

Yu, H. T., and L. Khazanovich, "Effects of constructions curling on concrete pavement behavior," *7th International Conference on Concrete Pavements*, Orlando, FL, September 2001, pp. 55-67.